ACS Photonics

Letter

pubs.acs.org/journal/apchd5

Asymmetric Light Absorption and Reflection in Freestanding Nanostructured Metallic Membranes

Serkan Butun and Koray Aydin*

Department of Electrical Engineering and Computer Science, Northwestern University, Evanston, Illinois 06202, United States

Supporting Information

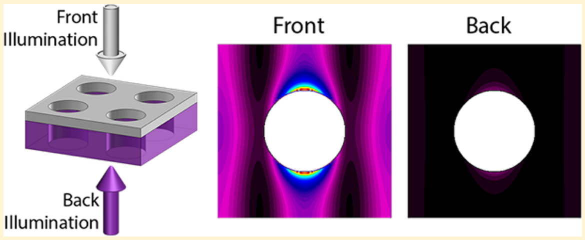

ABSTRACT: Resonant light absorption in metallic nanostructures results from highly localized electric fields that are crucial for many processes such as Raman scattering, photoluminescence, hot-carrier creation, and photovoltaics. In recent years, there have been a substantial amount of studies related to the design and realization of resonant optical absorbers from microwave to optical frequencies. However, there has been little thought that went into investigation of direction-dependent absorption and reflection characteristics of optical materials. In this study, we introduce and realize an absorber that is capable of absorbing light asymmetrically depending on the illumination direction. By designing an asymmetrical dielectric permittivity profile along the propagation direction, we have been able to control the optical resonance strength of the absorber, resulting in asymmetric light absorption and reflection at resonance wavelengths. The proposed structure consists of a square hole lattice etched into a free-standing Si_3N_4/Ag bilayer of total thickness 200 nm. A 9-fold front to back absorption contrast was measured with the fabricated structures, whereas a 13-fold contrast was achieved in finite difference time domain simulations. Moreover, mode profiles of observed resonances were discussed in detail to understand the physical mechanism of the asymmetric light absorption. Our analyses indicate that the same resonance modes were excited regardless of the illumination direction; however the coupling strength is greatly reduced when the structure is illuminated from the dielectric side. Asymmetric light absorbers and reflectors introduced here could find applications in energy-harvesting applications, particularly for photovoltaics and thermophotovoltaics.

KEYWORDS: *plasmonics, nanostructures, absorbers, metamaterials, metasurfaces*

There is a tremendous interest in optical absorbers among researchers and engineers to realize superior materials that can convert the energy in light to other usable forms such as electricity, heat, and mechanical energy. Semiconductors are traditionally the material of choice for light absorption; however, their absorption highly depends on their band gap, which rather limits their abilities in terms of tuning the position and the bandwidth of the absorption. On the other hand, resonant light absorption by means of nanostructured materials, so-called "metamaterials", allows the precise control of the absorption band in terms of both position and bandwidth. Furthermore, high material and fabrication cost makes semiconductors less desirable for most applications, whereas constituents of the metamaterials are often selected from earth-abundant metals and dielectrics, which are much cheaper. As a consequence of using subwavelength metallic structures as a building block of metamaterials, it is the excitation of surface plasmon resonances that causes highly localized electric fields. This phenomenon sparked a wide range of application possibilities such as photovoltaics,[1−5] surface-enhanced spectroscopy,[6−12] thermal detectors,[13,14] heat-assisted data recording,[15,16] and hot electron collectors.[17−20] Recently, considerable effort has been devoted to low-dimensional metamaterials, which are referred to as "metasurfaces", that have numerous functionalities using plasmonic building blocks such as radiative cooling,[21,22] spectrum splitting,[23−25] photo/thermovoltaics,[26−30] engineered thermal emission/absorption,[31,32] and artificial black materials.[33−35] Here we report on a free-standing membrane, an asymmetric absorber, which operates in the visible spectrum. Its absorption is a strong function of both the wavelength and the direction of illumination. While resonances of localized and propagating nature that are dictated by geometric parameters of the structure determine the position of the absorption band, the illumination direction governs the amplitude. This directionally dual-accessible design may find its use in applications such as directional heating/cooling. In addition, the small footprint of the structure is well-suited to all optical integrated circuits as a passive component. Although we have targeted the visible spectrum in this study, the concept can be scaled up to longer wavelengths as well as further down to the UV region by using Al as a plasmonic material. In principle, by using refractory materials such as tungsten as a metal and durable ceramics as dielectrics[36,37] it is possible to design an asymmetric absorber and thermal emitter for physically demanding environments.

Received: July 9, 2015
Published: November 16, 2015

DOI: 10.1021/acsphotonics.5b00377
ACS Photonics 2015, 2, 1652−1657

RESULTS AND DISCUSSION

Our asymmetric absorber consists of a square hole lattice made out of a bilayer metal/dielectric freestanding membrane. This design allows illumination from both directions. Due to the nature of the perforated metallic film, various types of optical resonances are excited, such as surface plasmon polaritons, localized surface plasmons, and waveguiding modes. Having optically different types of materials on two sides of the structure causes different optical resonances depending on the direction of illumination. Although similar designs were previously proposed and demonstrated by many in the context of enhanced transmission through subwavelength holes after the pioneering work by Ebbesen et al.,[38,39] the absorption aspect for realizing functional devices still remains unexploited. Figure 1 represents the structure of the proposed membrane. It consists of a square hole lattice fabricated on a Ag/Si_3N_4 (50/150 nm) membrane. Ag is chosen because its plasma edge is more suitable for our spectrum of interest. The plasma edge of the other commonly used metal Au makes it barely usable for this work. We define a front illumination direction when the structure is illuminated from the Ag side, as shown in Figure 1a. Likewise, the back illumination direction is defined as when the light is incident from the Si_3N_4 side. The design parameter set included the thicknesses of both Ag and Si_3N_4 layers, hole diameter, and the periodicity of the lattice (Figure 1b). We kept the periodicity in the x and y direction equal in order to eliminate the polarization dependence. We have fabricated these structures on commercially available Si_3N_4 membranes (see Methods). Two micrographs from both sides of the chip are presented in Figure 1c,d. Nine different designs can be seen on each micrograph. The white region in Figure 1c is the blank Ag film on top of the chip surface, whereas on the back side (Figure 1d) a green cast due to the S_3N_4 on the Si substrate is visible. The structures can be seen on the bottom of the trenches. Due to the asymmetric optical response, structures appear dimmer when observed from the front side of the chip, while they appear brighter when they are observed from the back side of the chip relative to the surrounding. A cross-sectional oblique SEM image in Figure 1e shows the fabricated bilayer free-standing Ag/Si_3N_4 membrane. This image displays a close-up view of an edge of an alignment feature next to the nanohole array. These features are fabricated with the nanohole array; therefore they are etched all the way through, as well. Figure 1f represents a close-up image from the Ag side of the fabricated square hole lattice. Due to the grainy nature of the evaporated Ag film, there is an inevitable degradation from the perfect hole geometry. We have taken this form deformation into account in our finite-difference time domain (FDTD) simulations later. In addition, Ag is known to oxidize quickly. Therefore, we performed our measurements as soon as possible after Ag deposition. Samples started to degrade in a week, which gave us enough time to complete the measurements.

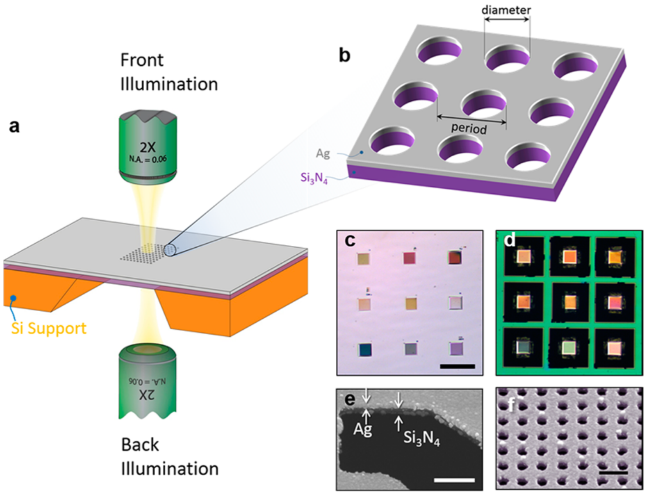

Figure 1. Schematic representation of our proposed asymmetric absorber. (a) The structure with two separate illumination configurations front and back. The fabricated ultrathin membrane is supported by a Si substrate. The illuminator objective (2×, NA 0.06) is placed either above or below the sample for front or back illumination cases, respectively. (b) Close-up schematics of the asymmetric absorber with indicated relevant design parameters. (c, d) Front and back view micrographs of a fabricated chip with nine different absorbers. The scale bar is 300 μm. (e) A 45° tilted SEM image of an edge of an alignment feature near the nanohole array revealing the bilayer membrane. The scale bar is 500 nm (note that the scale bar is in the horizontal direction, and the length is contracted along the vertical direction due to the tilt of the SEM). (f) Close up oblique angle SEM image of the fabricated freestanding membrane. The scale bar is 400 nm.

We have performed spectral reflectance and transmission measurements of the fabricated structures. Results are illustrated in Figure 2a and b, respectively. There is a significant change in the reflection curves with respect to the illumination direction. However, a negligible difference is observed in the transmission curves. The experimental absorption is then calculated using the formula $A = 1 - R - T$, where A, R, and T are absorption, reflection, and transmission, respectively. As can be seen in Figure 2c, there is a substantial difference in absorption depending on the illumination direction. The calculated contrast ratio (front to back) is 8-fold around both peak resonances 580 and 730 nm for this particular structure with periodicity 350 nm, and the hole diameter is 170 nm. We have performed FDTD simulations using digitized SEM images of the fabricated structures in order to address the discrepancies between the simulated perfect structures and the fabricated samples. Figure 2d shows the exact digitized simulation of the measured structure with 2 × 2 unit cell. We have randomly chosen a 2 × 2 region on the SEM image and fed it to our FDTD solver. Note that each hole in the fabricated lattice is unique. Moreover, it is not practical to simulate the entire structure, as it would require an unprecedented amount of computation capacity. Therefore, we attributed the small mismatch between two calculated and measured spectra to the structural differences in both cases. Nevertheless, there is a good agreement between the calculated and the measured absorption spectra. An additional comparison of absorption spectra to a hypothetical freestanding Ag layer with and without the nanostructured hole array is presented in supporting content Figure S1 to draw attention to the effectiveness of the Ag/Si_3N_4 heterostructure.

In order to investigate the effect of periodicity, we have fabricated asymmetric absorbers with 400 nm periodicity, as well. Measured front to back contrast ratios of 350 and 400 nm structures are compared in Figure 3a. Both modes are red-shifted by 70 nm each compared to the 350 nm periodicity structure. In addition, the measured contrast ratio is changing with respect to periodicity. The contrast ratio for both modes stayed around 8-fold in the 350 nm structure, whereas it is over

DOI: 10.1021/acsphotonics.5b00377
ACS Photonics 2015, 2, 1652−1657

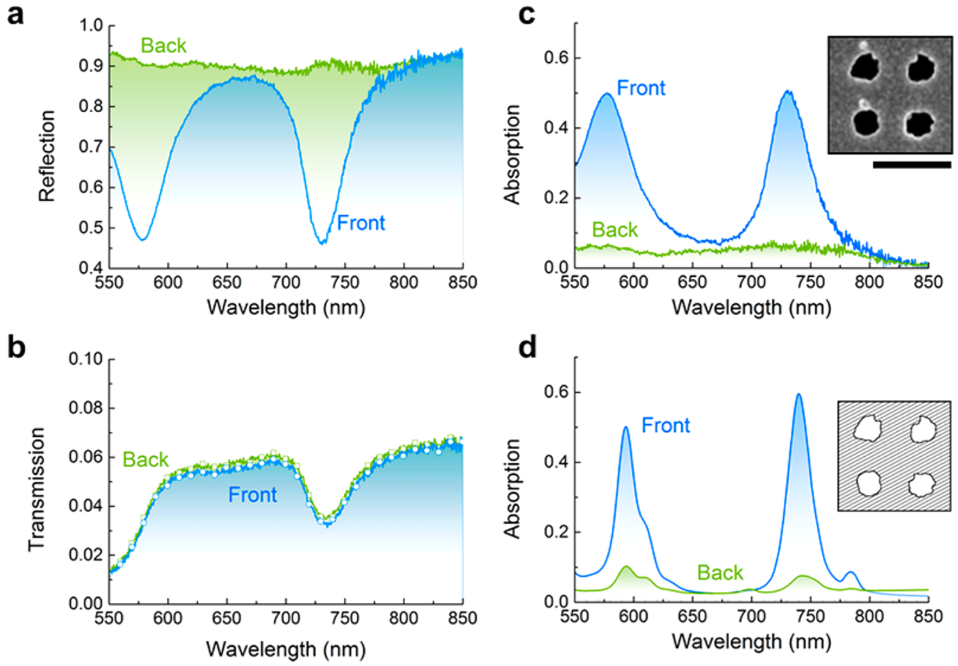

Figure 2. (a, b) Spectral reflection and transmission measurements of the asymmetric absorber. (c) Experimental spectral absorption curves of the fabricated asymmetric absorber for front and back illumination. Inset: Close-up SEM image of the measured structure. The scale bar is 400 nm. (d) Corresponding FDTD simulation of the measured structure. Inset: Unit cell used in FDTD calculations, which is obtained by digitizing the SEM image given in the inset of part a.

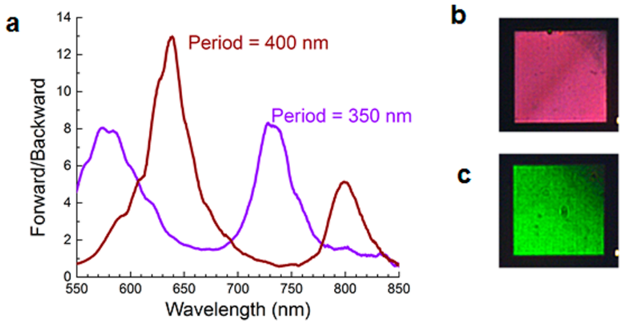

Figure 3. (a) Ratio of the measured front absorption to the back absorption for two different periodicities. (b, c) Optical images of the fabricated membranes in transmission mode for 350 and 400 nm periodicity structures, respectively.

13-fold for the first mode and about 5-fold for the second mode in the 400 nm structure.

Optical microscope images in transmission mode (Figure 3b,c) show the color-filtering behavior of Ag nanohole arrays, which is well understood.[40] Transmission bands around 400 and 540 nm for the structures shown in Figure 3b and c cause them to appear violet and green, respectively.

We have utilized the commercially available Lumerical FDTD solver for parameter optimization and to get insight into the nature of resonances and their dependence on structural parameters as well as the illumination direction. Although each structural parameter such as layer thicknesses and the diameter of holes has an effect on the performance, the periodicity is the most crucial one. Figure 4a,b represent the periodicity sweep for top and back illumination cases, respectively. All of the resonant modes red-shift with increasing periodicity. This suggests that all of the modes that are in this spectral region are propagating modes along the structure. Modes are more prominent when the structure is front illuminated. Furthermore, no spectral shift was observed depending on the illumination direction. We have plotted line cuts from periodicity sweeps to illustrate clearly the difference in absorption depending on the illumination in Figure 4c. For front illumination, absorption at 590 nm is about 60%, whereas it reaches 80% at 730 nm. In contrast, when the light is incident from the back side, absorption is drastically reduced to about 10% and 5% at corresponding wavelengths. The calculated front to back ratio reveals about 5-fold and 10-fold front to back absorption contrast for modes m_1 and m_2, respectively. The contrast is related with the resonance strength difference in each case. The m_2 mode is a quadrupole resonance when front and back illuminated. However, the m_1 mode is a dipole resonance in both front and back illumination cases. Due to the coupling strength difference in each case, the absorption contrast is lower in the m_2 mode in comparison to the m_1 mode. Further discussion on modes is provided below. Experimental front to back contrast data (Figure 3a) differ slightly in amplitude from FDTD calculations. We attribute this discrepancy mostly to structural imperfection aroused during the fabrication and the fact that it is not possible to incorporate the fabricated structure fully into the FDTD solver. In addition, measured contrast ratio amplitudes of modes m_1 and m_2 deviated from those in simulations, as we expect the amplitude of m_1 should be greater than m_2 regardless of the periodicity. This discrepancy is attributed to the poor signal-to-noise ratio of our measurement setup in the long-wavelength regime due to the reduced optical power and lower sensitivity of our CCD detector. Although we can measure a decent amplitude in the front illumination case, we cannot measure the back illumination case accurately because of the high noise level compared to the signal.

Time reversal symmetry is preserved, as the structure does not involve any hyperbolic or magnetooptic materials. This can be seen in Figure 4d, wherein we plot the calculated spectral

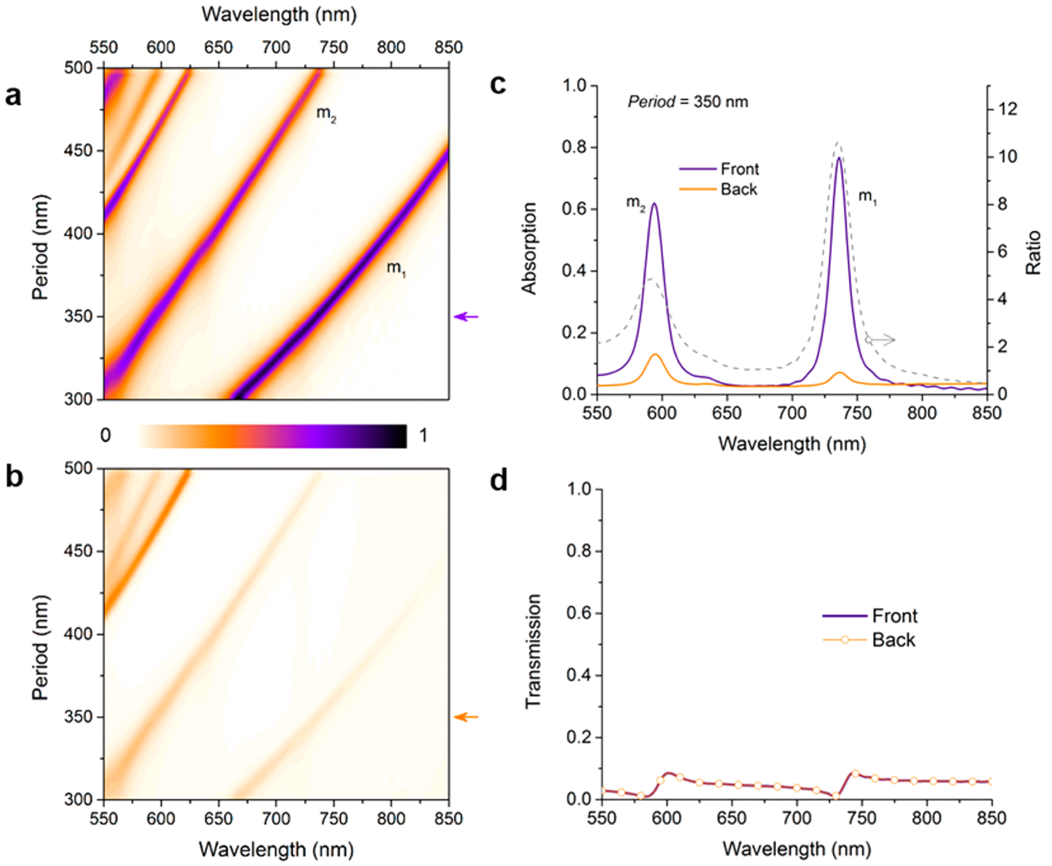

Figure 4. FDTD optimization of the asymmetric absorbers. (a, b) Periodicity sweep for a fixed hole diameter of 100 nm for top and back illumination, respectively. The color bar indicates the total absorption in both figures. Arrows at 350 nm periodicity indicate the positions of comparative line cuts shown in c. The ratio of both curves (front/back) is represented by the gray dashed line on the right y-axis. (d) Transmission data from the same periodicity. Due to the time reversal symmetry, both front and back transmission curves overlap.

transmission of the same 350 nm periodicity sample. Both front and back curves perfectly overlap, indicating the preservation of time reversal symmetry. The same behavior was also observed in transmission measurements, as shown in Figure 2b.

In order to gain physical insight into the absorption process, we have investigated mode profiles by analyzing 3D absorption maps calculated via FDTD simulations. Absorption as a function of wavelength at each point in space is calculated by the following:

$$A(\vec{r}, \lambda) = \frac{\varepsilon_0 c\pi}{\lambda} |\vec{E}(\vec{r}, \lambda)|^2 \ \varepsilon''(\vec{r}, \lambda) \tag{1}$$

where scalar quantities ε_0, c, λ, and ε'' are the permittivity of the free space, the speed of light, wavelength, and the imaginary part of the dielectric permittivity; vector quantities $\vec{r}$ and $\vec{E}$ are the position and the electric field, respectively. The absorption occurs largely at the Ag/Si_3N_4 interface. Therefore, absorption maps only at this interface are plotted here in Figure 5. Vertical cross-sectional absorption maps are provided in supporting content Figure S2. To draw a more comprehensive picture, absorption maps are embedded in 3D sketches. As per eq 1, there is no absorption where ε'' is zero. Hence all of the light is absorbed inside the Ag film. Figure 5a–d show the absorption distribution at modes m$_1$ and m$_2$ for illumination directions both front and back. The higher absorption (Figure 4a,c) m$_1$ mode has dipolar characteristics as shown in Figure 5c, which is the fundamental electrical mode along the polarization direction and is allowed by the coupling of the grating

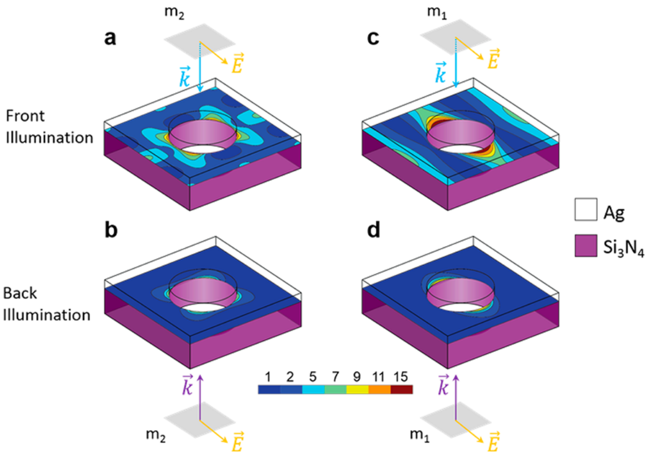

Figure 5. Calculated absorption profiles in the unit cell of the absorber as a function of both wavelength and illumination direction. Absorption of the Ag/Si_3N_4 interface where most of the incident light is absorbed is presented. (a, b) m$_2$ mode front and back illumination configuration, respectively. (c, d) m$_1$ mode in front and back illumination configuration, respectively. Patch colors represent relative intensity in all figures. In (b) and (d), absorption is scaled up by 20 times for a better visual representation.

momentum of only one dimension, whereas the quadrupole nature m$_2$ mode (Figure 5a) is the higher energy second-order electrical mode that is caused by the addition of grating momentum in both the x and y dimension.[39] The surface current density plots provided in Figure S3 in the supporting content further support the electrical nature of modes m_1 and m_2. The absorption maps for the back illumination case in Figure 5b,d also show similar character to the front illumination case. However, the intensity is much lower. Note that map data in Figure 5b and d are scaled up by 20 times to enhance the visibility. The lower Si_3N_4 layer reduces the coupling strength; therefore the total absorption in the back illumination case stays poor.

■ CONCLUSION

In conclusion, an ultrathin, freestanding asymmetric absorber of total thickness 200 nm based on a square hole lattice is designed, fabricated, and tested. Extensive FDTD calculations were conducted to optimize the structure and explain observed resonant modes in the spectrum. Spectral absorption measurements were carried out for the fabricated structures. Our absorber exhibited about a 13-fold experimental absorption front to back contrast ratio at the fundamental electrical resonance in simulations. The measured absorption contrast reached almost 9-fold for the same mode. In addition, realistic simulations performed with digitized SEM images helped explain the disagreement between calculated and observed absorption spectra. This proof of concept design can be utilized for various applications, where directional absorption and/or emission is desired such as all-optical integrated circuits.

■ METHODS

FDTD Simulations. FDTD simulations were performed by a commercial software package developed by Lumerical Inc. The dispersive material data of Ag Palik[41] and a constant refractive index of 2.1 were used for the Si_3N_4 layer. A mesh overwrite region of $1 \times 1 \times 1$ nm^3 was defined over the hole geometry. The boundary conditions in the *xy* and *z* directions were set as periodic and perfectly matched layers. The simulation software ensures numerical stability by setting the time step at less than 0.02 fs based on the chosen mesh sizes.

Metamaterial Fabrication. Structures were fabricated on commercially available 200 nm thick Si_3N_4 membranes. First, the membranes are etched down to 150 nm via a CF_4 + O_2 based reactive ion etching (RIE) process. Due to the severe etch rate difference between Si_3N_4 and Ag, it is not possible to pattern a Si_3N_4/Ag stack at once. Therefore, a sacrificial 30 nm Cr layer was deposited on the Si_3N_4 layer. We have used focused ion beam lithography to define our square hole patterns on the Cr layer. Subsequently, we transfer this pattern on the Si_3N_4 membrane using the same RIE process used to thin the membrane. The sacrificial Cr layer was removed by a wet Cr etchant standard (Sigma-Aldrich). Finally, a 50 nm Ag film was deposited on a perforated Si_3N_4 membrane using e-beam deposition.

Measurements. Spectral reflectance and transmittance measurements were carried out using an inverted microscope equipped with a spectrometer consisting of a 303 mm focal-length monochromator and an Andor Newton electron multiplication charge-coupled device camera. A broadband halogen lamp was used to generate a broadband illumination. Measurement area was set to an area of roughly 90×90 μm^2 using a 2× Nikon microscope objective with a numerical aperture of 0.06. The reflectance was calibrated with a broadband dielectric mirror (Edmund Optics #64-114) with an average reflection of 99% between 350 and 1100 nm. The transmittance was calibrated by free space.

■ ASSOCIATED CONTENT

Ⓢ Supporting Information

The Supporting Information is available free of charge on the ACS Publications website at DOI: 10.1021/acsphotonics.5b00377.

> Comparison of absorption with respect to perforated silver film without any dielectric and blank silver film, cross-sectional absorption maps in *xz* and *yz* planes, and surface current density plots (PDF)

■ AUTHOR INFORMATION

Corresponding Author

*E-mail: aydin@northwestern.edu.

Notes

The authors declare no competing financial interest.

■ ACKNOWLEDGMENTS

This material is based upon work supported by the AFOSR under Award No. FA9550-12-1-0280. K.A. acknowledges financial support from the McCormick School of Engineering and Applied Sciences at Northwestern University and partial support from the Institute for Sustainability and Energy at Northwestern (ISEN) through ISEN Equipment and Booster Awards. This research was also partially supported by the Materials Research Science and Engineering Center (NSF-MRSEC) (DMR-1121262) of Northwestern University. This research made use of the NUANCE Center at Northwestern University, which is supported by NSF-NSEC, NSF-MRSEC, Keck Foundation, and the State of Illinois and the NUFAB cleanroom facility at Northwestern University.

■ REFERENCES

(1) Novotny, L.; van Hulst, N. Antennas for light. *Nat. Photonics* **2011**, *5*, 83−90.

(2) Ferry, V. E.; Munday, J. N.; Atwater, H. A. Design Considerations for Plasmonic Photovoltaics. *Adv. Mater.* **2010**, *22*, 4794−4808.

(3) Solano, M. E.; Faryad, M.; Monk, P. B.; Mallouk, T. E.; Lakhtakia, A. Periodically multilayered planar optical concentrator for photovoltaic solar cells. *Appl. Phys. Lett.* **2013**, *103*, 191115.

(4) Gan, Q.; Bartoli, F. J.; Kafafi, Z. H. Plasmonic-Enhanced Organic Photovoltaics: Breaking the 10% Efficiency Barrier. *Adv. Mater.* **2013**, *25*, 2385−2396.

(5) Atwater, H. A.; Polman, A. Plasmonics for improved photovoltaic devices. *Nat. Mater.* **2010**, *9*, 205−213.

(6) Anker, J. N.; Hall, W. P.; Lyandres, O.; Shah, N. C.; Zhao, J.; Van Duyne, R. P. Biosensing with plasmonic nanosensors. *Nat. Mater.* **2008**, *7*, 442−453.

(7) Adato, R.; Altug, H. In-situ ultra-sensitive infrared absorption spectroscopy of biomolecule interactions in real time with plasmonic nanoantennas. *Nat. Commun.* **2013**, *4*, 2154.

(8) Yanik, A. A.; Cetin, A. E.; Huang, M.; Artar, A.; Mousavi, S. H.; Khanikaev, A.; Connor, J. H.; Shvets, G.; Altug, H. Seeing protein monolayers with naked eye through plasmonic Fano resonances. *Proc. Natl. Acad. Sci. U. S. A.* **2011**, *108*, 11784−11789.

(9) Cinel, N. A.; Bütün, S.; Ertaş, G.; Özbay, E. SERS: 'Fairy Chimney'-Shaped Tandem Metamaterials as Double Resonance SERS Substrates (Small 4/2013). *Small* **2013**, *9*, 489−489.

(10) Ayas, S.; Topal, A. E.; Cupallari, A.; Güner, H.; Bakan, G.; Dana, A. Exploiting Native Al2O3 for Multispectral Aluminum Plasmonics. *ACS Photonics* **2014**, *1*, 1313−1321.

(11) Abb, M.; Wang, Y.; Papasimakis, N.; de Groot, C. H.; Muskens, O. L. Surface-Enhanced Infrared Spectroscopy Using Metal Oxide Plasmonic Antenna Arrays. *Nano Lett.* **2014**, *14*, 346−352.

(12) Law, S.; Yu, L.; Rosenberg, A.; Wasserman, D. All-Semiconductor Plasmonic Nanoantennas for Infrared Sensing. *Nano Lett.* **2013**, *13*, 4569−4574.

(13) Zhang, F.; Shen, Q.; Shi, X.; Li, S.; Wang, W.; Luo, Z.; He, G.; Zhang, P.; Tao, P.; Song, C.; Zhang, W.; Zhang, D.; Deng, T.; Shang, W. Infrared Detection Based on Localized Modification of Morpho Butterfly Wings. *Adv. Mater.* **2015**, *27*, 1077−1082.

(14) Yi, F.; Zhu, H.; Reed, J. C.; Cubukcu, E. Plasmonically Enhanced Thermomechanical Detection of Infrared Radiation. *Nano Lett.* **2013**, *13*, 1638−1643.

(15) Kryder, M. H.; Gage, E. C.; McDaniel, T. W.; Challener, W. A.; Rottmayer, R. E.; Ganping, J.; Hsia, Y.-T.; Erden, M. F. Heat Assisted Magnetic Recording. *Proc. IEEE* **2008**, *96*, 1810−1835.

(16) Stipe, B. C.; Strand, T. C.; Poon, C. C.; Balamane, H.; Boone, T. D.; Katine, J. A.; Li, J.-L.; Rawat, V.; Nemoto, H.; Hirotsune, A.; Hellwig, O.; Ruiz, R.; Dobisz, E.; Kercher, D. S.; Robertson, N.; Albrecht, T. R.; Terris, B. D. Magnetic recording at 1.5 Pb m-2 using an integrated plasmonic antenna. *Nat. Photonics* **2010**, *4*, 484−488.

(17) Chalabi, H.; Schoen, D.; Brongersma, M. L. Hot-Electron Photodetection with a Plasmonic Nanostripe Antenna. *Nano Lett.* **2014**, *14*, 1374−1380.

(18) Li, W.; Valentine, J. Metamaterial Perfect Absorber Based Hot Electron Photodetection. *Nano Lett.* **2014**, *14*, 3510−3514.

(19) Knight, M. W.; Sobhani, H.; Nordlander, P.; Halas, N. J. Photodetection with Active Optical Antennas. *Science* **2011**, *332*, 702−704.

(20) Manjavacas, A.; Liu, J. G.; Kulkarni, V.; Nordlander, P. Plasmon-Induced Hot Carriers in Metallic Nanoparticles. *ACS Nano* **2014**, *8*, 7630−7638.

(21) Shi, J.; Liu, B.; Li, P.; Ng, L. Y.; Shen, S. Near-Field Energy Extraction with Hyperbolic Metamaterials. *Nano Lett.* **2015**, *15*, 1217−1221.

(22) Rephaeli, E.; Raman, A.; Fan, S. Ultrabroadband Photonic Structures To Achieve High-Performance Daytime Radiative Cooling. *Nano Lett.* **2013**, *13*, 1457−1461.

(23) Ni, X.; Emani, N. K.; Kildishev, A. V.; Boltasseva, A.; Shalaev, V. M. Broadband Light Bending with Plasmonic Nanoantennas. *Science* **2012**, *335*, 427.

(24) Black, L.-J.; Wang, Y.; de Groot, C. H.; Arbouet, A.; Muskens, O. L. Optimal Polarization Conversion in Coupled Dimer Plasmonic Nanoantennas for Metasurfaces. *ACS Nano* **2014**, *8*, 6390−6399.

(25) Clausen, J. S.; Højlund-Nielsen, E.; Christiansen, A. B.; Yazdi, S.; Grajower, M.; Taha, H.; Levy, U.; Kristensen, A.; Mortensen, N. A. Plasmonic Metasurfaces for Coloration of Plastic Consumer Products. *Nano Lett.* **2014**, *14*, 4499−4504.

(26) Lenert, A.; Bierman, D. M.; Nam, Y.; Chan, W. R.; Celanovic, I.; Soljacic, M.; Wang, E. N. A nanophotonic solar thermophotovoltaic device. *Nat. Nanotechnol.* **2014**, *9*, 126−130.

(27) Chen, X.; Chen, Y.; Yan, M.; Qiu, M. Nanosecond Photothermal Effects in Plasmonic Nanostructures. *ACS Nano* **2012**, *6*, 2550−2557.

(28) Rinnerbauer, V.; Lenert, A.; Bierman, D. M.; Yeng, Y. X.; Chan, W. R.; Geil, R. D.; Senkevich, J. J.; Joannopoulos, J. D.; Wang, E. N.; Soljačić, M.; Celanovic, I. Metallic Photonic Crystal Absorber-Emitter for Efficient Spectral Control in High-Temperature Solar Thermophotovoltaics. *Adv. Energy Mater.* **2014**, *4*, 1400334.

(29) Wu, C.; Neuner, B., III; John, J.; Milder, A.; Zollars, B.; Savoy, S.; Shvets, G. Metamaterial-based integrated plasmonic absorber/emitter for solar thermo-photovoltaic systems. *J. Opt.* **2012**, *14*, 024005.

(30) Guo, Y.; Molesky, S.; Hu, H.; Cortes, C. L.; Jacob, Z. Thermal excitation of plasmons for near-field thermophotovoltaics. *Appl. Phys. Lett.* **2014**, *105*, 073903.

(31) Kocer, H.; Butun, S.; Li, Z.; Aydin, K. Reduced near-infrared absorption using ultra-thin lossy metals in Fabry-Perot cavities. *Sci. Rep.* **2015**, *5*, 8157.

(32) Streyer, W.; Law, S.; Rooney, G.; Jacobs, T.; Wasserman, D. Strong absorption and selective emission from engineered metals with dielectric coatings. *Opt. Express* **2013**, *21*, 9113−9122.

(33) Aydin, K.; Ferry, V. E.; Briggs, R. M.; Atwater, H. A. Broadband polarization-independent resonant light absorption using ultrathin plasmonic super absorbers. *Nat. Commun.* **2011**, *2*, 517.

(34) Spinelli, P.; Hebbink, M.; de Waele, R.; Black, L.; Lenzmann, F.; Polman, A. Optical Impedance Matching Using Coupled Plasmonic Nanoparticle Arrays. *Nano Lett.* **2011**, *11*, 1760−1765.

(35) Butun, S.; Aydin, K. Structurally tunable resonant absorption bands in ultrathin broadband plasmonic absorbers. *Opt. Express* **2014**, *22*, 19457−19468.

(36) Li, W.; Guler, U.; Kinsey, N.; Naik, G. V.; Boltasseva, A.; Guan, J.; Shalaev, V. M.; Kildishev, A. V. Refractory Plasmonics with Titanium Nitride: Broadband Metamaterial Absorber. *Adv. Mater.* **2014**, *26*, 7959−7965.

(37) Guler, U.; Boltasseva, A.; Shalaev, V. M. Refractory Plasmonics. *Science* **2014**, *344*, 263−264.

(38) Ebbesen, T. W.; Lezec, H. J.; Ghaemi, H. F.; Thio, T.; Wolff, P. A. Extraordinary optical transmission through sub-wavelength hole arrays. *Nature* **1998**, *391*, 667−669.

(39) Ghaemi, H. F.; Thio, T.; Grupp, D. E.; Ebbesen, T. W.; Lezec, H. J. Surface plasmons enhance optical transmission through subwavelength holes. *Phys. Rev. B: Condens. Matter Mater. Phys.* **1998**, *58*, 6779−6782.

(40) Yokogawa, S.; Burgos, S. P.; Atwater, H. A. Plasmonic color filters for CMOS image sensor applications. *Nano Lett.* **2012**, *12*, 4349−54.

(41) Palik, E. D. *Handbook of Optical Constants of Solids.*; Academic Press, 1998.

DOI: 10.1021/acsphotonics.5b00377